Lidar Observation of Elevated Pollution Layers over Los Angeles*

ROGER M. WAKIMOTO

Department of Atmospheric Sciences, University of California, Los Angeles, CA 90024

JAMES L. McELROY

U.S. Environmental Protection Agency, Environmental Monitoring Systems Laboratory, Las Vegas, NV 89114

(Manuscript received 25 January 1986, in final form 26 April 1986)

ABSTRACT

Elevated pollution layers are observed over Los Angeles with an aircraft equipped with a downward-looking lidar. For the first time, detailed ancillary upper-air kinematic and thermodynamic data were collected simultaneously to aid in the interpretation of these elevated layers. It is concluded that upper-level winds within the inversion, orographic effects, and thermally induced changes in the depth of the mixed layer control the evolution of these layers.

1. Introduction

Los Angeles has frequently been a subject of air pollution studies owing to its unique meteorological setting and related air quality problems. The key feature is the persistent elevated temperature inversion (Robinson, 1952; Edinger, 1959) which is, to a large extent, a result of the large-scale subsidence and light winds associated with the semipermanent Pacific High. This subsidence produces an air mass which is relatively warm and dry, except within the lower atmosphere where a thin marine layer (~300–600 m in depth) has evolved with the temperature and humidity characteristics of the sea surface over which it has been moving for many days. The boundary between these air masses is marked by the strong (~7–9°C) temperature inversion that suppresses large-scale convection and reduces vertical mixing. Consequently, air contaminants produced in the Los Angeles area are trapped near or at the surface. It should be noted that this climatological situation is not unique to Los Angeles. Cities such as Casablanca, Capetown and Lima are also extremely vulnerable to smog (Neiburger, 1969).

Another dominant feature over Los Angeles are the local winds which are strongly influenced by two factors: 1) the local alteration between the sea breeze blowing toward the land (ocean) during the day (night), and 2) the thermally induced mountain–valley breezes and the orographically induced obstacle flows (Beer and Leopold, 1947). In addition, there is an urban heat island effect; however, Schultz and Warner (1982) have concluded that its influence is relatively small.

Many previous studies concentrated on the transport of pollutants below the marine inversion. The extensive surface wind network within the Los Angeles area has been used to estimate surface air trajectories to determine probable sources of the pollutants responsible for high concentrations in specific local regions, e.g., Kauper (1960). In subsequent years, constant volume balloons (tetroons) were released from various sites for the purpose of estimating the three-dimensional air trajectories in the low levels over the basin (Holzworth et al., 1963; Pack and Angell, 1963; Angell et al., 1972, 1975, 1976). More recent work has utilized chemical tracer releases as a means of identifying possible pollutant paths in and around the Los Angeles area (Drivas and Shair, 1974; Lamb et al., 1978). However, until recently there has been relatively little effort to study the vertical distribution of pollutants within the stable layer above the base of the temperature inversion. These "elevated pollution layers" are important to understand (e.g., their origins, the depth AGL, etc.), since the contaminants trapped within them may be fumigated to lower levels during the same day or on subsequent days as the boundary layer deepens owing to convective thermals generated by surface heating. This deepening in turn causes a more rapid buildup of pollutant concentrations at the surface than might be expected (Blumenthal et al., 1978). Such fumigation may occur near the origin of the elevated layer or at another location depending on the kinematics of the boundary layer wind structure.

* The research described in this article has been funded in part by the United States Environmental Protection Agency but it has not been subjected to agency review; therefore it does not necessarily reflect the views of the agency and no official endorsement should be inferred.

One of the first studies on elevated pollution layers was by Lea (1968), documenting maximum ozone concentrations above the base of the inversion. Edinger and Helvey (1961) and Edinger et al. (1972) had speculated that these elevated layers might exist and suggested two mechanisms for their formation:

1) local convergence zones caused by the alteration of the sea breezes around complex topography; and
2) orographically assisted convection over heated mountain slopes that weaken the inversion and pump pollutants aloft (sometimes referred to as the "chimney-effect").

Owing to the sparseness of surface and upper-air observations, these hypotheses could not be confirmed until LIDAR (LIght Detection And Ranging) was developed and subsequently applied to air quality and meteorological studies in the boundary layer (e.g., Hamilton, 1966; Collis, 1969; Johnson, 1969; Johnson and Uthe, 1971; Uthe and Russell, 1974; Uthe and Wilson, 1979; Uthe et al., 1980a; McElroy et al., 1981; Shipley et al., 1984; Uthe, 1984; and Melfi et al., 1985). In particular, lidar has been demonstrated to be capable of detecting the distribution of the particulate pollution and attendant boundary layer structure in the atmosphere with high spatial and temporal resolution. Recent studies in the Los Angeles area using downward-looking lidar aboard aircraft (Uthe et al., 1980b; McElroy, 1982; McElroy, 1985) revealed the existence of elevated aerosol layers above the base of the temperature inversion. Such layers were attributed to heated upslope flow in conjunction with wind shear aloft, air mass convergence in complex terrain, and undercutting of one air mass by another of different density (e.g., the sea breeze).

Unfortunately, these recent studies lacked detailed ancillary upper-air kinematic and thermodynamic data essential to confirm speculations concerning the origin and evolution of such elevated layers. This paper is a first attempt to quantitatively describe vertical lidar observations of elevated pollution layers over Los Angeles using high-resolution data collected during Project BASIN (Basic Studies on Airflow, Smog and the INversion) (Wakimoto and Wurtele, 1984).

Project BASIN, a mesometeorological project over Los Angeles which was the data source for this research paper, is discussed in section 2. The synoptic and mesoscale conditions during the analysis periods are described in section 3. The lidar and supplementary surface and upper-air data for several times are shown and analyzed in section 4. Discussion and conclusions drawn from the analysis are presented in section 5.

2. Project BASIN, the data source

In the summer of 1984, the most comprehensive collection of air quality and meteorological data ever attempted over Los Angeles was directed by the University of California at Los Angeles (UCLA), with the aid and cooperation of several organizations listed in Wakimoto and Wurtele (1984). Overall and enlarged base maps of the BASIN network are shown in Figs. 1 and 2, respectively. A dense network of surface stations recording wind speed and direction, temperature, and dewpoint temperature information was deployed during the project. In addition to these parameters, South Coast Air Quality Management District (SCAQMD) stations recorded gaseous air pollutant concentrations (e.g., ozone) on a continuous basis. During the field phase of BASIN, radiosondes and airsondes were launched every 4 h around the clock at 11 upper-air stations (Table 1) for three complete days of monitoring, consisting of the following periods:

1) 1300 GMT 8 August–1200 GMT 10 August;
2) 0000 GMT 18 August–2300 GMT 18 August (GMT = 8 hrs + PST).

An aircraft equipped with a downward-looking solid-state pulsed lidar was flown by the Environmental Protection Agency (EPA) to observe distributions of aerosol concentrations in the atmosphere. With the aerosol lidar, range-resolved atmospheric backscatter and surface-reflected energy (ground return) are obtained at the transmitted wavelengths. The laser signal returns are recorded in digital form by a magnetic tape recorder. On-board microprocessor systems allow the lidar data to be shown in real time on a television monitor as distance–height displays in shades of gray. Geographical positioning of data points is by a dedicated Loran C navigational system. Details concerning the lidar system are contained in McElroy et al. (1982) and McElroy and Smith (1986). Two of the lidar flight transects, labeled A and B in Figs. 1 and 2, are discussed and interpreted in this paper using surface and upper-air observations collected during BASIN. Transect A was flown between 2200 and 2229 GMT on 9 August and transect B was flown between 0308 and 0334 GMT on 10 August.

3. Synoptic and mesoscale conditions

The synoptic conditions from 8 to 10 August were typical for southern California in the summer. The axis of a strong ridge at the 500 mb level (not shown) was centered over the coastline on 8 August and subsequently drifted eastward, in response to a short-wave trough approaching the Pacific Northwest, and was located over Eastern Nevada, Idaho and western Montana by 10 August. Although this movement of the ridge might suggest an end to the large-scale subsidence, the height of the 500 mb surface at Vandenberg Air Force Base and San Diego, California, did not change, remaining at ~5900 geopotential meters (gpm) for the entire period.

At the lower levels (not shown), the synoptic flow was dominated by the Pacific High located offshore,

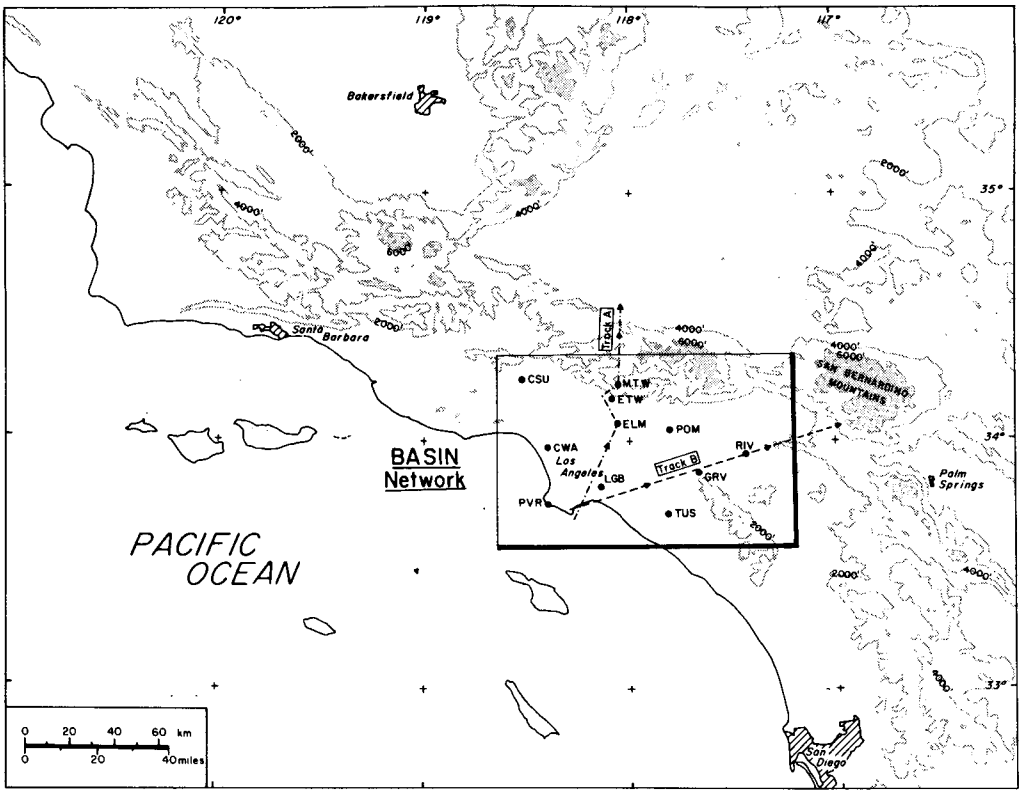

FIG. 1. The BASIN network located over southern California. The dashed line and the dash-dot line delineate flight paths of the Environmental Protection Agency (EPA) lidar aircraft. The 11 upper-air sites are listed in Table 1. The boxed-in area is enlarged in Fig. 2.

with north to northwesterly winds along the coast of California, and the thermally induced low pressure area over the desert regions in the extreme southwestern United States and northern Mexico. The thermal low in conjunction with the Pacific High produces an onshore component enhancing the sea breeze during the day. Based on the above observations, a pollution episode had been predicted to occur by the SCAQMD (Joe Cassmassi, personal communication, 1984), for the entire operational period.

The mesoscale conditions on 8 August were influenced by a very strong low-level inversion owing to the synoptic situation on these 3 days. An ~10°C inversion at ~900 mb, as measured at Long Beach, is shown in Fig. 3. At 2100 GMT (Fig. 4a), the sea breeze is apparent over the entire basin with high ozone concentrations farther inland. A peak ozone value of 29 parts per hundred million (pphm) was reported near Pasadena (see Fig. 2) at this time; this value is one considered to be "unhealthful for everyone" by the SCAQMD (e.g., South Coast Air Quality Management District, 1985). By 0500 GMT 9 August (Fig. 4b), the sea breeze had weakened but there was still a west to east flow across Los Angeles. The air was relatively clean with all SCAQMD monitoring stations reporting ozone concentrations less than 5 pphm. The advection of ozone out of the Basin during the late afternoon and evening by the sea breeze is a common scenario over Los Angeles. In addition, ozone production locally drops dramatically after 1) suspension of nonshift related industrial activities; 2) the evening rush hour traffic is over; and 3) the sun sets on the horizon.

Although the synoptic scale conditions did not change significantly from 8 to 10 August, an interesting mesoscale feature developed over the ocean west of Los Angeles which altered the boundary layer structure over the Basin. The phenomenon is known as the "Catalina Eddy" (Rosenthal, 1968; Bosart, 1983; Dorman, 1985), so-called since it is an eddy circulation with its center located near Santa Catalina Island off the coast west of Los Angeles. It is typically 200 to 300 km in diameter and results in the development of southerly to southeasterly winds along the southern California coastal area. Although the recent work of Bosart (1983) and Dorman (1985) have clarified various aspects of the eddy, it is clear that the mechanism for its formation is still not completely understood.

Figure 4c (2100 GMT 9 August) illustrates the mesoscale influence of the eddy on the windflow patterns over Los Angeles. Examples of the wind field over a larger spatial scale during an eddy event are well illustrated by Bosart (1983; see his Figs. 4, 6 and 7). Mod-

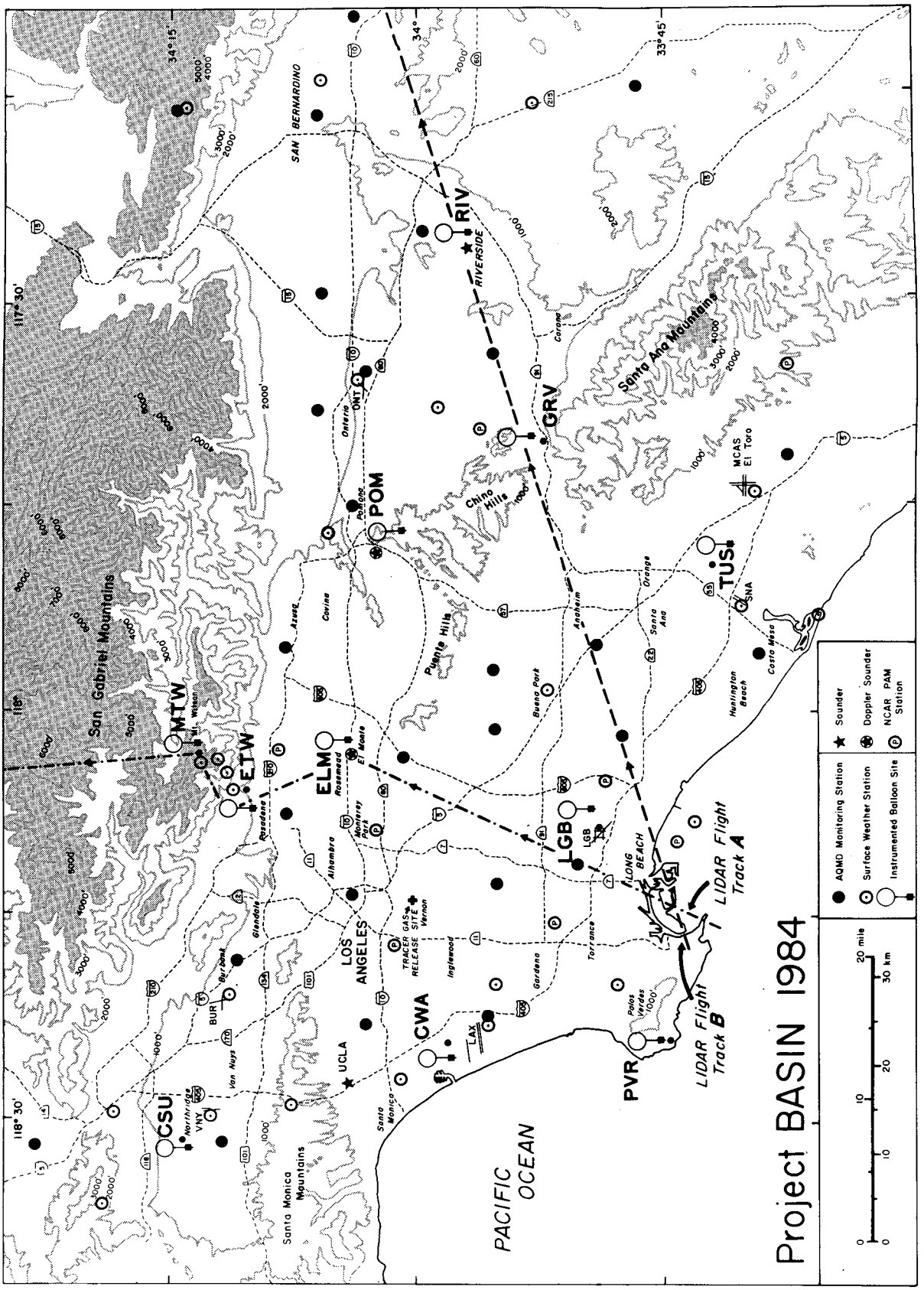

FIG. 2. An enlarged map of the BASIN network. The dashed line and the dash-dot line delineate flight paths of the EPA lidar aircraft.

TABLE 1. BASIN upper-air sites.

Identifier	Location	Elevation (m) MSL
CSU	California State University, Northridge	295
CWA	Cowan Ave	47
ELM	El Monte	76
ETW	Eaton Wash Dam	280
GRV	Green River Golf Course	146
LGB	Long Beach Airport	16
MTW	Mount Wilson Observatory	1725
POM	Pomona	207
PVR	Palos Verdes	105
RIV	Riverside Airport	244
TUS	Tustin	17

erate southerly winds are apparent except near Santa Monica and the Los Angeles International Airport (LAX) (see Fig. 2) where the sea breeze forces the winds toward a more westerly component. In contrast to the previous day, the ozone concentrations have fallen dramatically. The important difference in the flow patterns at the surface in Figs. 4a, c is that, during the eddy event shown in Fig. 4c, the wind direction near the coastal regions south of Long Beach are not perpendicular to the coast (i.e., southwesterly), but are from a southeasterly direction. When the sea breeze weakened at night (Fig. 4d) the southerly flow prevailed over most of the Los Angeles Area.

The eddy has been observed to alter the structure of the boundary layer when it forms; in general, coastal visibilities improve and the marine layer deepens during the first night after its formation. Air pollutants presumably mix vertically and hence become diluted within the deeper marine layer with resulting transport through mountain passes out of the Basin. This deepening is shown in Fig. 3 by the time sequence of soundings launched at LGB. Although it is beyond the scope of this paper, a detailed analysis of the Catalina Eddy during Project BASIN is currently underway.

4. Lidar cross sections

This section presents two lidar cross sections labeled A and B in Figs. 1 and 2 along with the wind, temperature and humidity data collected at the upper-air sites along the flight path. Unfortunately, owing to mechanical problems aboard the aircraft, only one pass over each track was flown; therefore, time continuity is lacking in this presentation. To help in overcoming this lack of information, cross sections of the sounding data are presented and interpreted at times before the aircraft traverses.

a. Track A

The lidar data for track A is presented in Fig. 5. For each such flight transect, the lidar data are shown graphically as images in shades of gray with the strongest scatter black and the lightest one white. The heavy lines of strong scatter at the bottom of the images represent the ground return. The high concentration of particulate matter below the base of the inversion (the "mixed layer") is clearly evident in Fig. 5a. The attenuation of the laser beam to a point where the ground is barely detectable on the left side of Fig. 5a is caused by a deck of stratus clouds. Note the change in the boundary layer structure as the marine air ascends via forced and/or free convection (thermals) up the heated slope of the San Gabriel Mountains. Although the boundary layer appears to be thinner along the slope of the mountain, the actual depth, perpendicular to the mountain slope, is ~3 km, owing to the vertical-scale distortion of the data presentation. However, the boundary layer is decreasing in depth relative to the Z coordinate reaching a minimum at ~850 mb. This lidar observation would explain the maximum in surface ozone concentration noted by Edinger (1973) at approximately the same level on other mountain slopes; i.e., at a height two-thirds to three-quarters up the mountain slope.

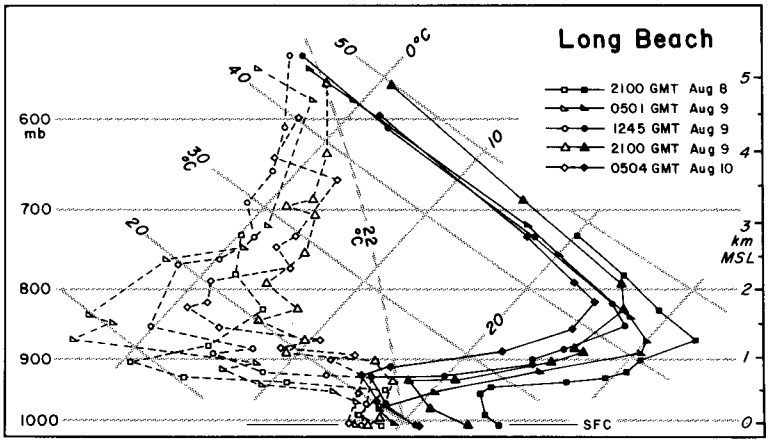

FIG. 3. Radiosonde soundings launched at Long Beach (LGB) from 8 to 10 August 1984. Solid lines are temperatures and dashed lines are dewpoint temperatures.

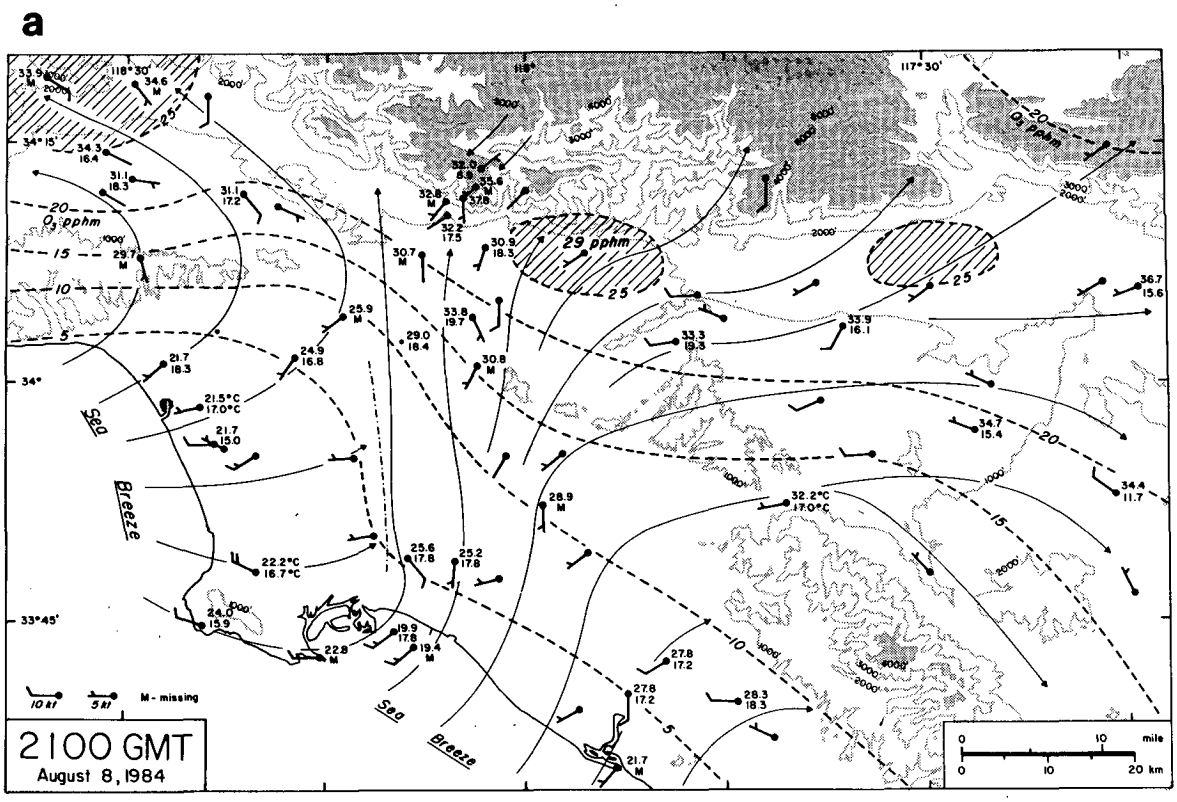

FIG. 4a. Surface airflow pattern and ozone concentrations for 2100 GMT 8 August 1984. The dashed lines are ozone concentrations in parts per hundred million (pphm). Solid lines are streamlines.

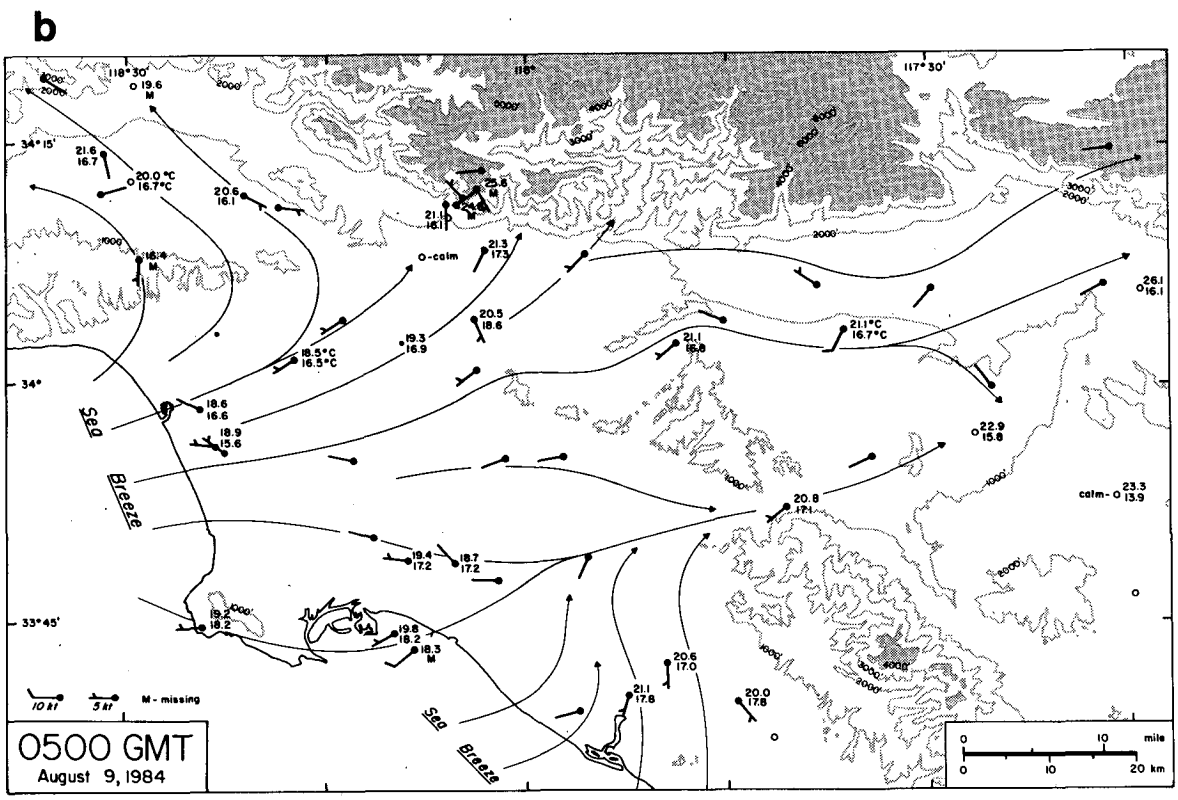

FIG. 4b. As in Fig. 4a except for 0500 GMT 9 August 1984.

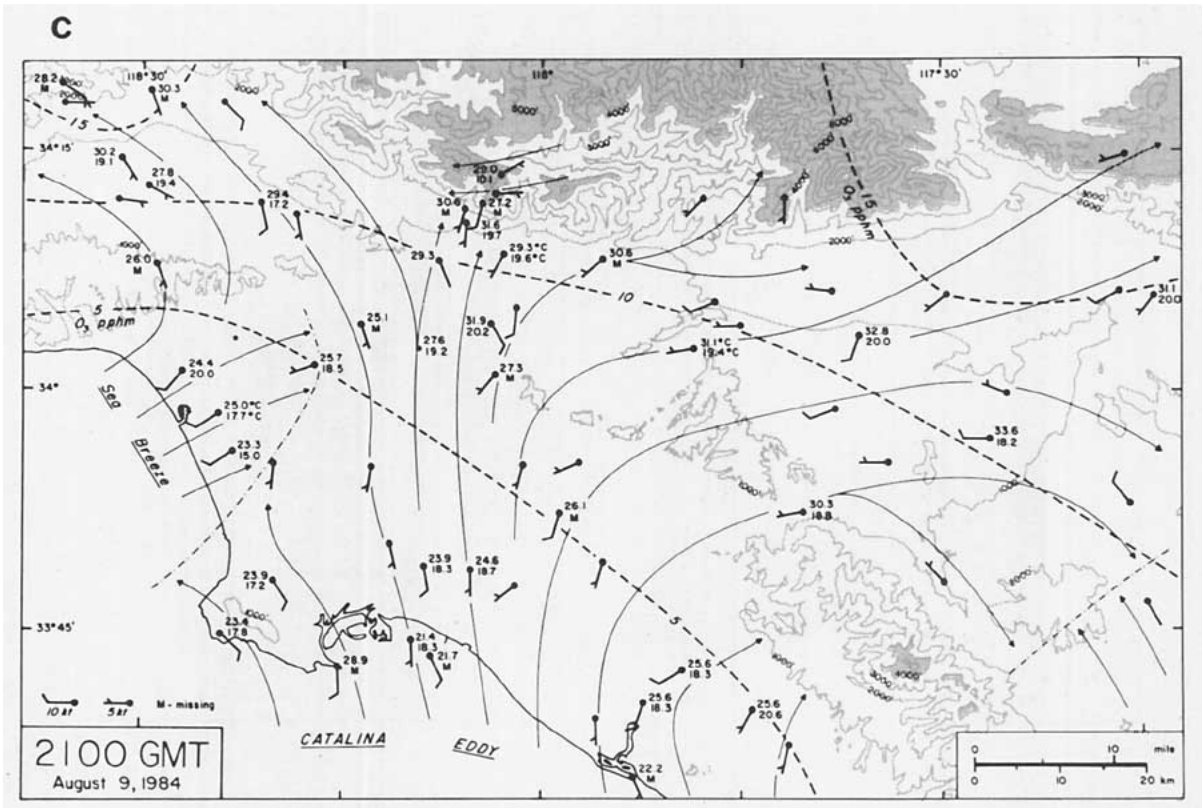

FIG. 4c. As in Fig. 4a except for 2100 GMT 9 August 1984.

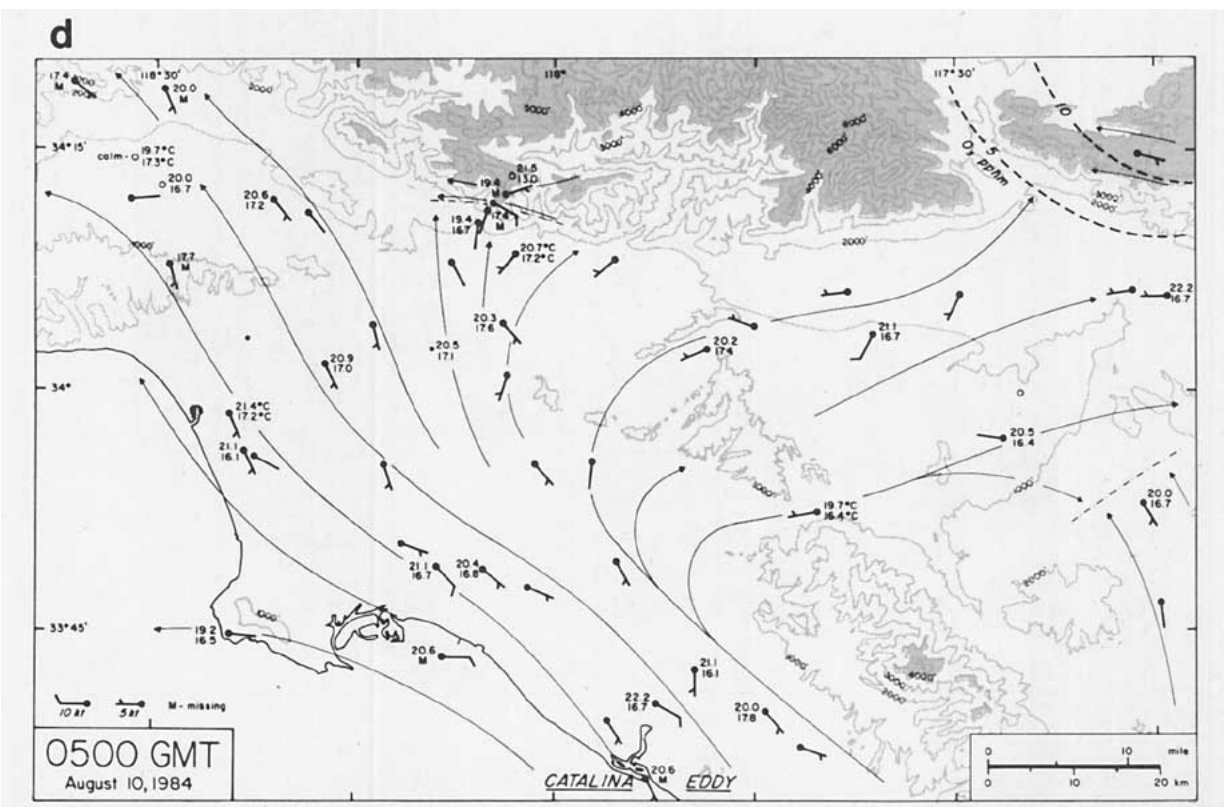

FIG. 4d. As in Fig. 4a except for 0500 GMT 10 August 1984.

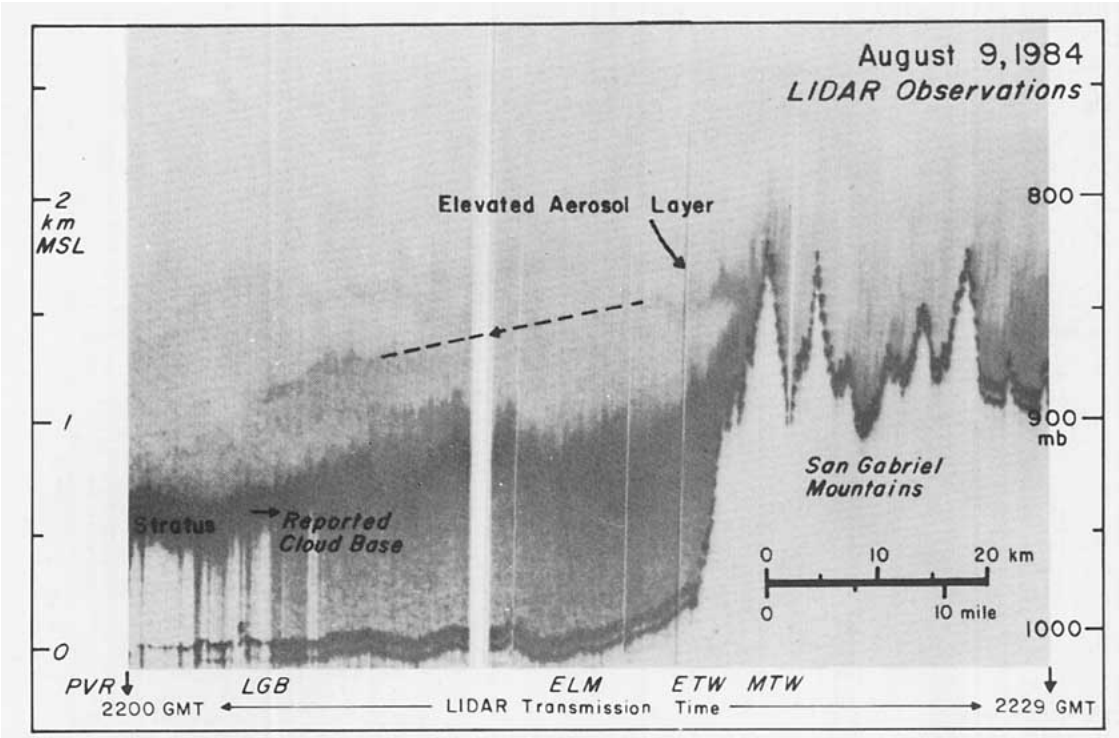

5a

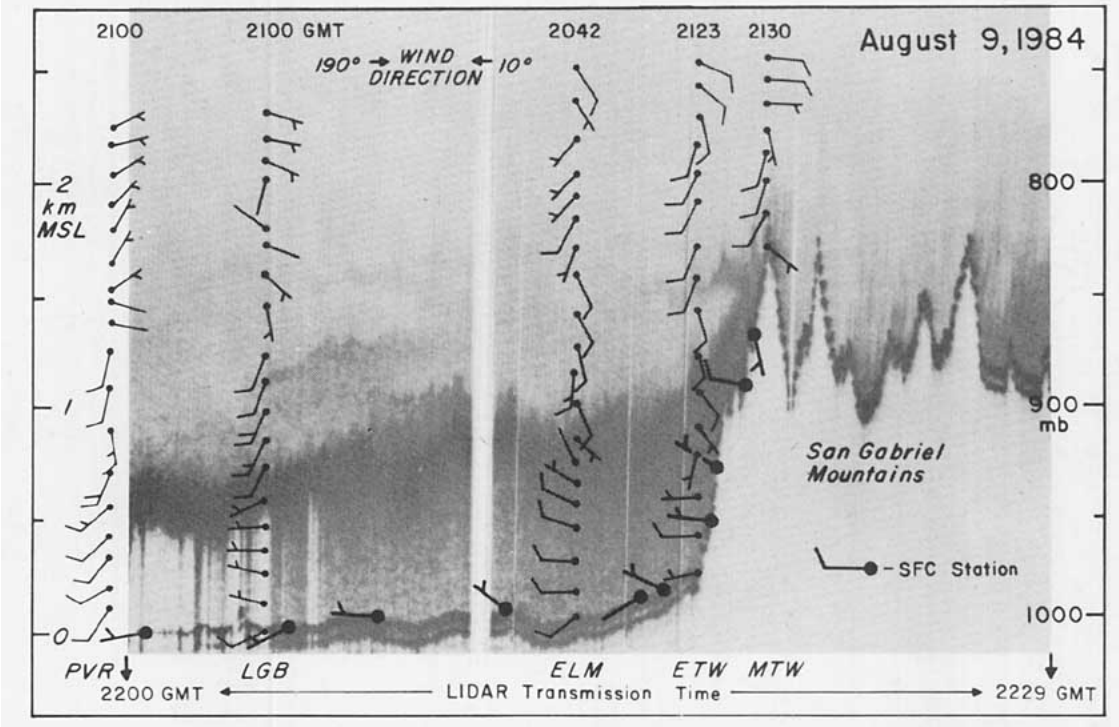

5b

FIG. 5. Lidar cross section over track A (a) without superimposed data; (b) with surface and upper-level winds superimposed; (c) with potential temperature and ozone concentrations superimposed; and (d) with relative humidity superimposed. Balloons were launched at the five upper-air sites (PVR, LGB, ELM, ETW and MTW) at ~2100 GMT 9 August 1984. The dashed line in Fig. 5a indicates that the two elevated aerosol layers may be contiguous. Wind speeds are in knots. Lidar data are gray scale representations of aerosol backscatter of laser signal at 0.532 μm.

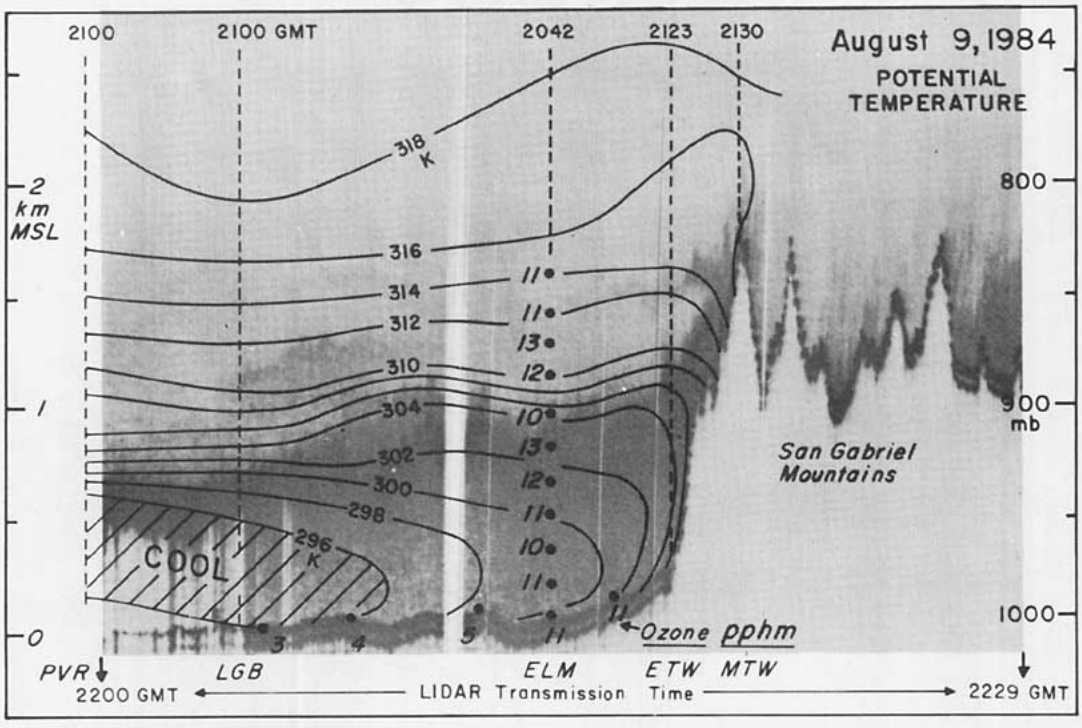

5c

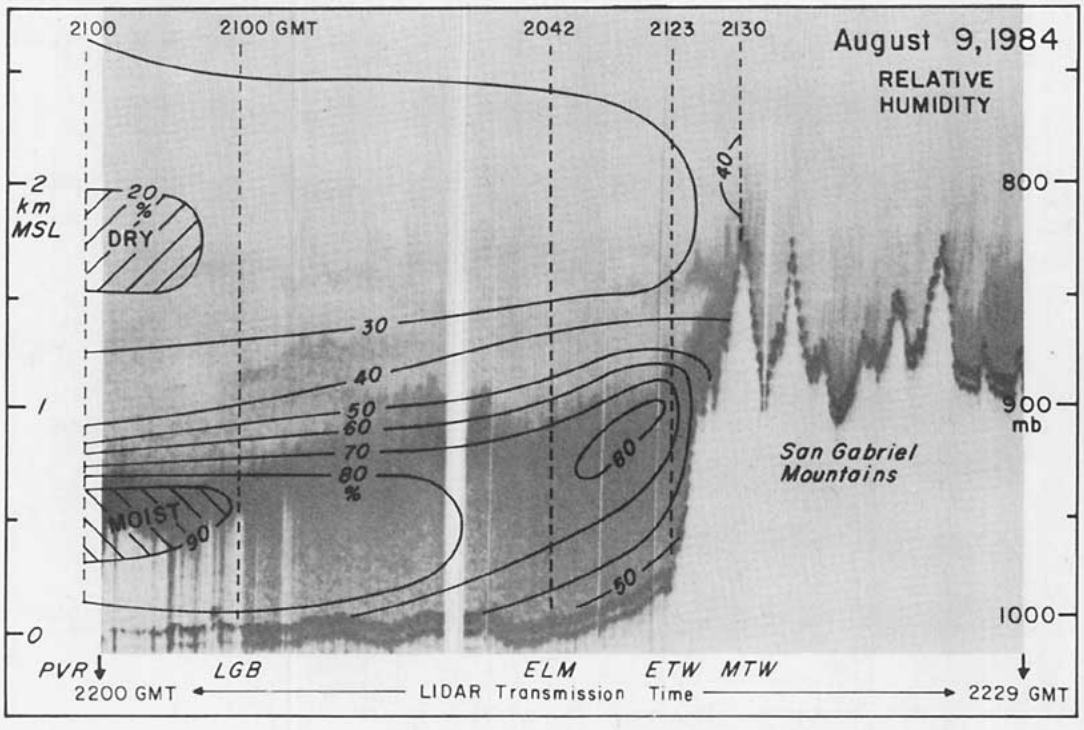

5d

FIG. 5. (*Continued*)

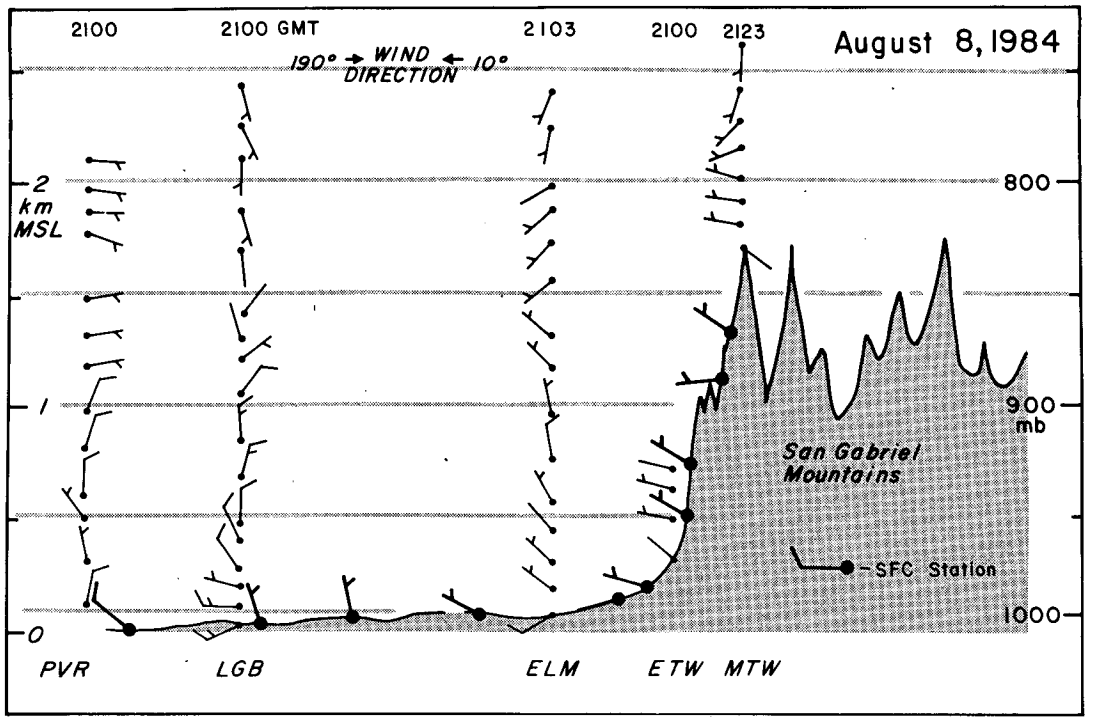

a

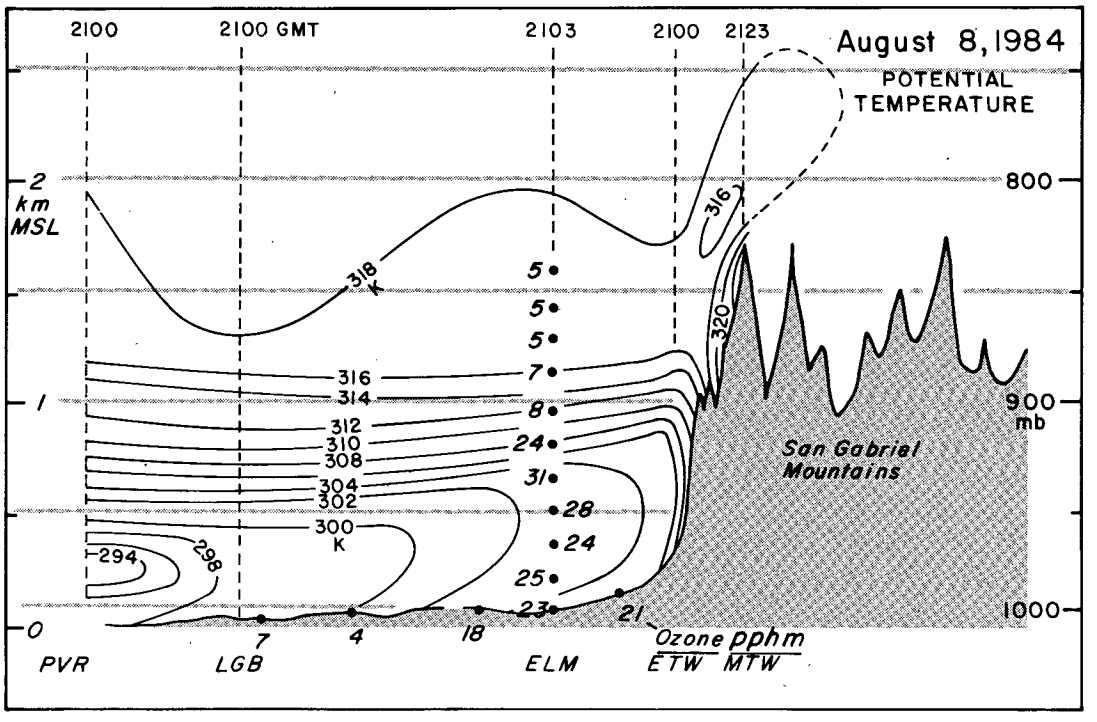

b

FIG. 6. Vertical cross sections of (a) surface and upper-level wind field; (b) potential temperature and ozone concentrations; and (c) relative humidity field for the same track as in Fig. 5 at ~2100 GMT 8 August 1984.

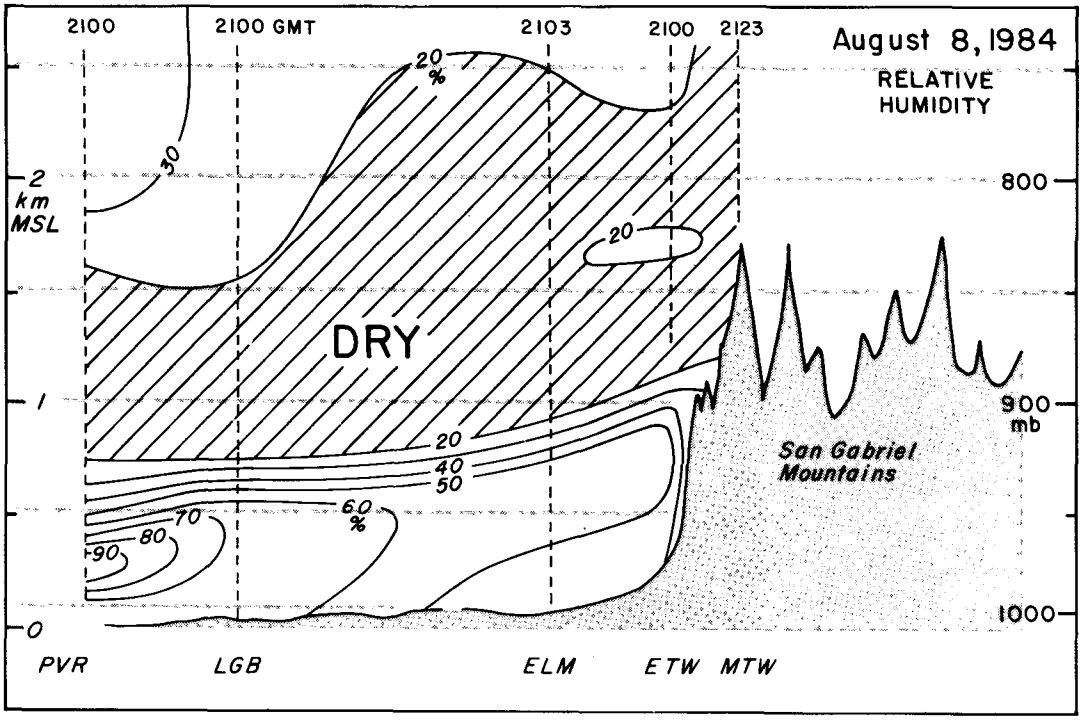

C

FIG. 6. (*Continued*)

Although not totally apparent in the pictorial display of the gray scale representation of the lidar data in Fig. 5a, the two elevated aerosol layers above the mixed layer are believed to be contiguous as indicated by the dashed line. This hypothesis is supported by subsequent analyses. Figure 5a is similar to pictures shown by Uthe et al. (1980b) of the pollution structure over Los Angeles; however, in the present study, five upper-air sites (labeled on the figure) were collecting data along the flight path.

The wind information for the 2100 GMT launch from PVR, LGB, ELM, ETW and MTW are plotted on Fig. 5b. The surface flow field in Fig. 4c supports an analysis along this cross section since the flow is nearly parallel to this section except near the top of Mt. Wilson, where the flow becomes easterly. Strong southerly flow below the inversion within the mixed layer is contributing to the upslope flow. This southerly flow is continuous up the mountain slope until ~870 mb, where the surface station depicts an easterly wind, and at the top of Mt. Wilson, where the station recorded a northerly wind. This change in wind direction is consistent with the location of the elevated aerosol layer flowing southward away from the slope leading up to Mt. Wilson. It should be mentioned that the pollutants depicted within the elevated aerosol layer likely originated from an area east of the cross section presented in Fig. 5 since the winds within this layer are from an easterly direction.

Figure 5c is a potential temperature analysis corresponding to the lidar cross section. The base of the inversion is denoted by the 296 K isentrope over PVR since it marks the boundary of a rapid vertical increase of potential temperature. The base rises to higher levels as the air moves inland toward the mountains. The deepening is mainly a result of the modification of the marine layer by the convection produced by heating of the ground (Edinger, 1963). The air is unstable near the mountain slopes and is characterized by nearly vertical isentropes. This potential temperature analysis is similar to ones presented by Defant (1951), Malkus (1955), Cramer and Lynott (1961), Orville (1964, 1968), Fosberg (1967) and Cramer (1972). Figures 5b, c suggest that the rising motion up the mountain slope, as shown by the lidar images, is a combination of forced (by the southerly flow) and thermally induced upslope flow (owing to the heating of the mountain slope).

The analysis in Fig. 5c suggests that a weak stable layer whose base is denoted by the 312 K isentrope acted as the "lid" for the elevated aerosol layer. Fortunately, a vertical profile of ozone concentration was measured in situ by an instrumented aircraft at ~2030 GMT over ELM (see Fig. 5c). There is a drop in ozone as the aircraft penetrates the base of the first inversion (denoted by the 304 K isentrope) and a subsequent rise and fall as the aircraft passes the base of the second stable layer (denoted by the 312 K isentrope). These

observations support the continuity of the elevated pollution layer indicated by the dashed line in Fig. 5a.

At this point it should be mentioned that the depiction of such aerosol layers by lidar does not necessarily imply that the gaseous pollutants are also contained at elevated concentrations. In fact, the lidar may be monitoring the aerosol mass associated with gaseous pollutants, especially secondary ones. Blumenthal et al. (1978) have shown that the vertical distribution of light-scattering aerosols is well correlated to that of ozone except in the early morning hours. They state that most of the light-scattering aerosols in Los Angeles smog are a product of atmospheric reactions which form secondary pollutants like ozone. Therefore, the correlation between the light-scattering coefficient and ozone concentrations is consistent with the hypothesis that the aerosol is a by-product of the photochemical reactions which yield ozone.

An analysis of the relative humidity distribution is shown in Fig. 5d. The presence of stratus is supported by the high relative humidity values on the left side of the figure. As the air moves up the mountain slope an increase in relative humidity occurs as air parcels expand and cool. The "pumping" of moisture above Mt. Wilson is illustrated by the 40% isohume.

It is apparent from the deepening of the marine layer shown in Fig. 3 that the mesoscale conditions on 9 August were strongly influenced by the Catalina Eddy. Therefore, it should be determined whether the observations shown in Fig. 5 are unique or whether these profiles could be observed on days when the meteorological conditions were more typical of a heavy smog episode. To attempt to resolve this issue, an analysis of the sounding data from the previous day was performed even though lidar data were not available (Fig. 6). Recall that at the surface, the airflow patterns at 2100 GMT on these two days did not appear to be substantially different (compare Figs. 4a and 4c).

In Fig. 6a, the winds within the mixed layer are similar to those in Fig. 5b; however, the winds aloft exhibit a more westerly component. The wind information from the mountain surface stations are approximately the same on both days (note that the northerly wind at MTW is similar to Fig. 5b). The major differences between 8 August and 9 August occur in the potential temperature fields; the inversion on 8 August is stronger and lower. The vertical profile of ozone concentration does not indicate a secondary peak aloft owing to the lack of a corresponding elevated inversion; therefore an elevated aerosol layer may not have been present. The heating of the mountain slope is still evident and, combined with the southerly flow in the mixed layer, apparently is advecting substantial quantities of pollutants aloft. However, in the absence of an elevated inversion and with an upper-level wind field which does not support a "return flow" over the Basin, most of the pollutants were dispersing well above the mountains. It should be noted that the 2100–2130 GMT time may be too early in the afternoon for the upslope/return flow to be fully developed. Unfortunately, the next launch time (0100 GMT) is too late to observe the return flow. In Fig. 6c, the strength of the inversion is shown by the very rapid drop in relative humidity above its base.

b. Track B

The lidar data collected when the aircraft passed over track B are presented in Fig. 7. Perhaps more dramatically than in Fig. 5, elevated pollution layer structure is clearly indicated over RIV and GRV. A qualitative description based on Fig. 7a suggests that the low-level inversion has dissipated at GRV with an apparent abrupt increase in mixing height at this location. From GRV eastward, the mixing height relative to the surface decreases, particularly over the mountain slopes. Similar to Fig. 5, there appears to be a pronounced orographic effect in the generation of the elevated pollution layer. It is interesting to note that although the air is relatively clean near the surface at GRV and RIV (ozone concentrations of 2–3 pphm), there apparently is extensive pollution aloft. Unfortunately, no vertical profiles of ozone concentrations were available at this time.

An interesting feature shown in Fig. 7 is the wave-like structure (horizontal wavelength ~38 km) of the elevated aerosol layer. The upper-air and lidar observations are not complete enough to determine the nature of this wave; however, it may be an internal gravity wave. Unfortunately, linear theory supports internal disturbances of all wavelengths; thus, it is difficult to explain the presence of a wave with this particular length of scale.

A striking feature in Fig. 7b is the observation that the low-level inversion does not dissipate at GRV, as suggested by the lidar data alone, but is continuous to RIV. The westerly winds within the mixed layer are advecting pollutants eastward up the slope of the San Bernardino Mountains. The meteorological data support the contention that these pollutants are subsequently advected by the easterly winds aloft back over the basin at the ~860 to 870 mb level. The relative humidity analysis (Fig. 7c) supports the existence of a deeper boundary layer toward the eastern part of the basin.

In an attempt to understand the evolution of the lidar data shown in Fig. 7, the upper-air data for 2100 GMT 9 August was plotted and analyzed (Fig. 8).[1] It becomes apparent after examining Fig. 8 that although the low-level inversion was continuous from GRV to RIV in Fig. 7b earlier in the day, the mixed layer was deeper owing to thermal convection caused by surface heating and extended to ~900 mb between GRV and

[1] Unfortunately, the upper-air data for 0100 GMT 10 August were not complete, so the preceding launch time was chosen.

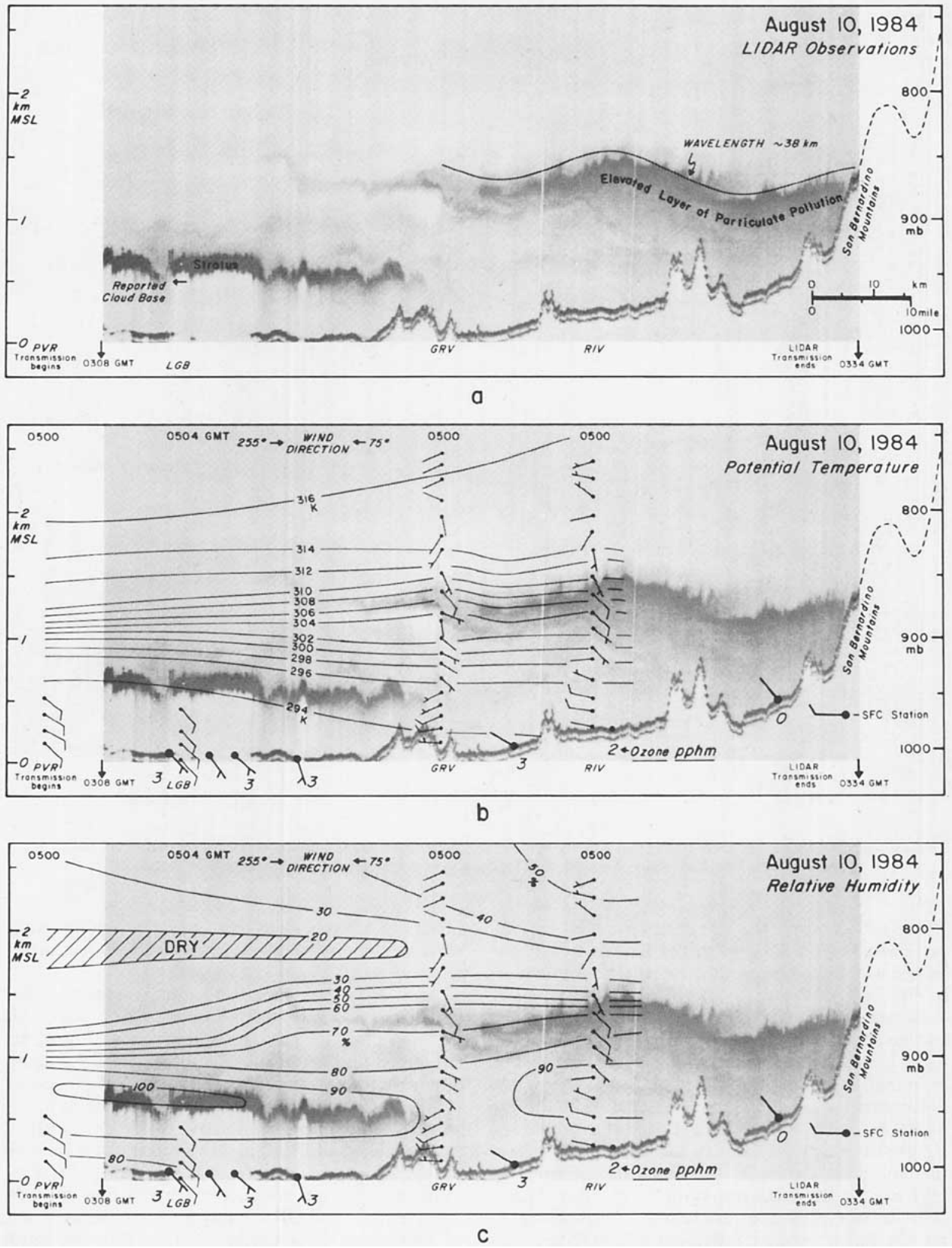

FIG. 7. Lidar cross section over track B (a) without superimposed data; (b) with surface and upper-level winds, potential temperature, and ozone concentrations superimposed; and (c) with surface and upper-level winds and relative humidity superimposed. Balloons were launched at the four upper-level sites (PVR, LGB, GRV and RIV) at ~0500 GMT 10 August 1984. Wind speeds are in knots. Lidar data are gray scale representations of aerosol backscatter of laser signal at 0.532 μm.

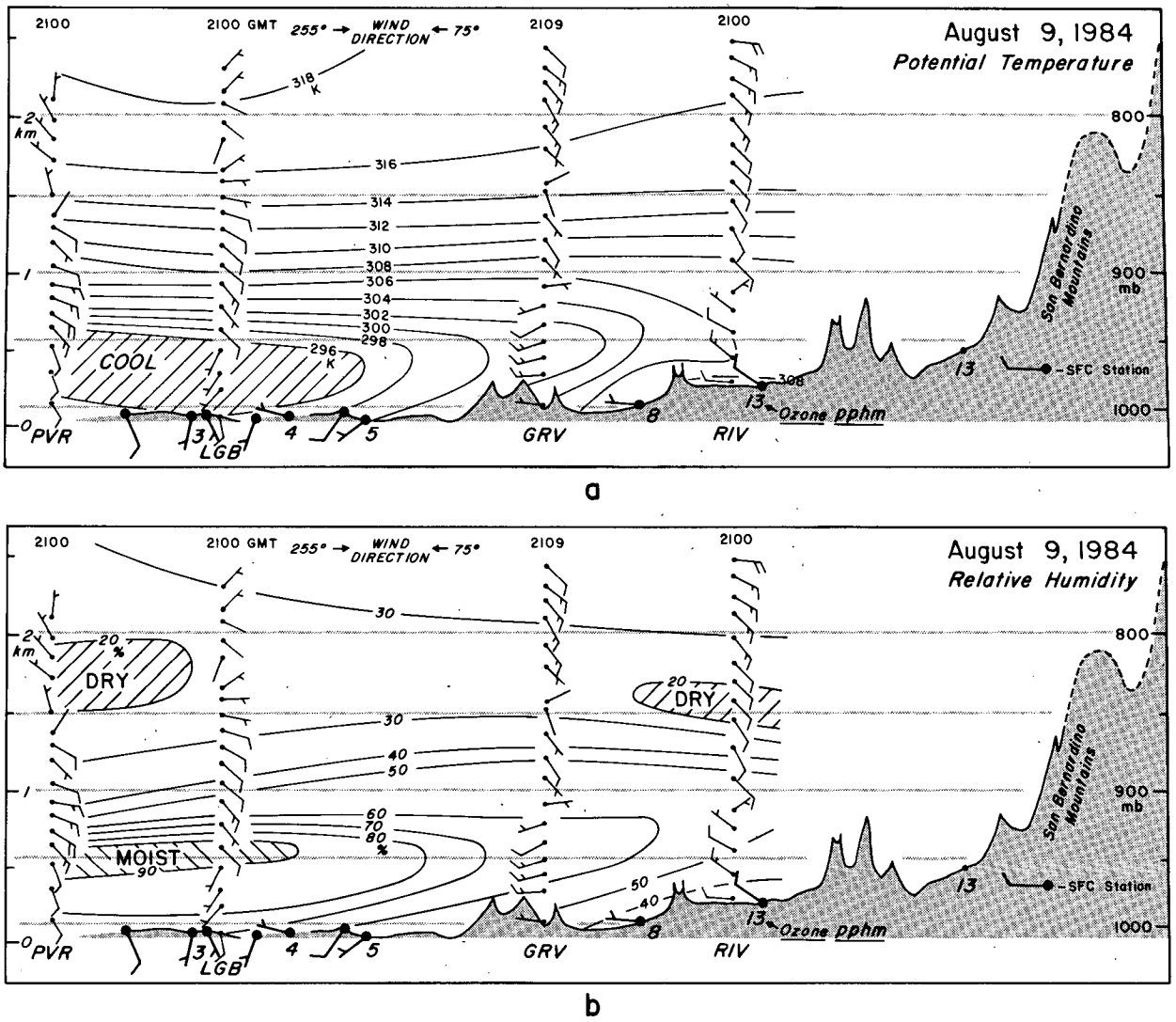

FIG. 8. Vertical cross section of (a) surface and upper-level wind field, potential temperature, and ozone concentration; (b) surface and upper-level wind field, and relative humidity field for the same track as in Fig. 7 at ~2100 GMT 9 August 1984.

RIV. The location of the base of the inversion over the east basin (~308 K isentrope) in Fig. 8a is well correlated with the position of the elevated pollution layer in Fig. 7.

Between the analysis times in Figs. 7 and 8, the land surface cooled and the base of the inversion began to lower to the position shown in Fig. 7b. In fact, a close examination of Fig. 7a shows that a faint layer of pollution exists at approximately the location of the 296 to 298 K isentrope. Russell et al. (1974) has discussed a probable reason for the poor depiction of the base of this inversion. During a subsidence regime when an inversion begins to develop or to lower, often there is little or no optical contrast between neighboring air masses. Lidar detection is delayed until sufficient particles are trapped below the inversion to define the interface. This process is just beginning in Fig. 7. The humidity pattern in Fig. 8b does not appear to be significantly different than that in Fig. 7c, although the relative humidity values are lower owing to the warmer temperatures.

As in subsection 4a, it is advantageous to compare conditions in Fig. 7 with those occurring before the Catalina Eddy formed. Accordingly, Fig. 9 was constructed from data obtained at 0500 GMT 9 August. Similar to the analysis presented in Fig. 6, the inversion is lower and stronger than on the following day. The westerly winds within and above the inversion would not appear to support the occurrence of an elevated pollution layer as dramatic as shown in Fig. 7. (However, there is some evidence of easterly flow at ~950 mb over RIV and GRV implying a possible existence of an elevated-layer structure.) It is likely that much of the pollution was advected through mountain passes and over the slopes of the San Bernardino Mountains by these winds. However, note the larger separation

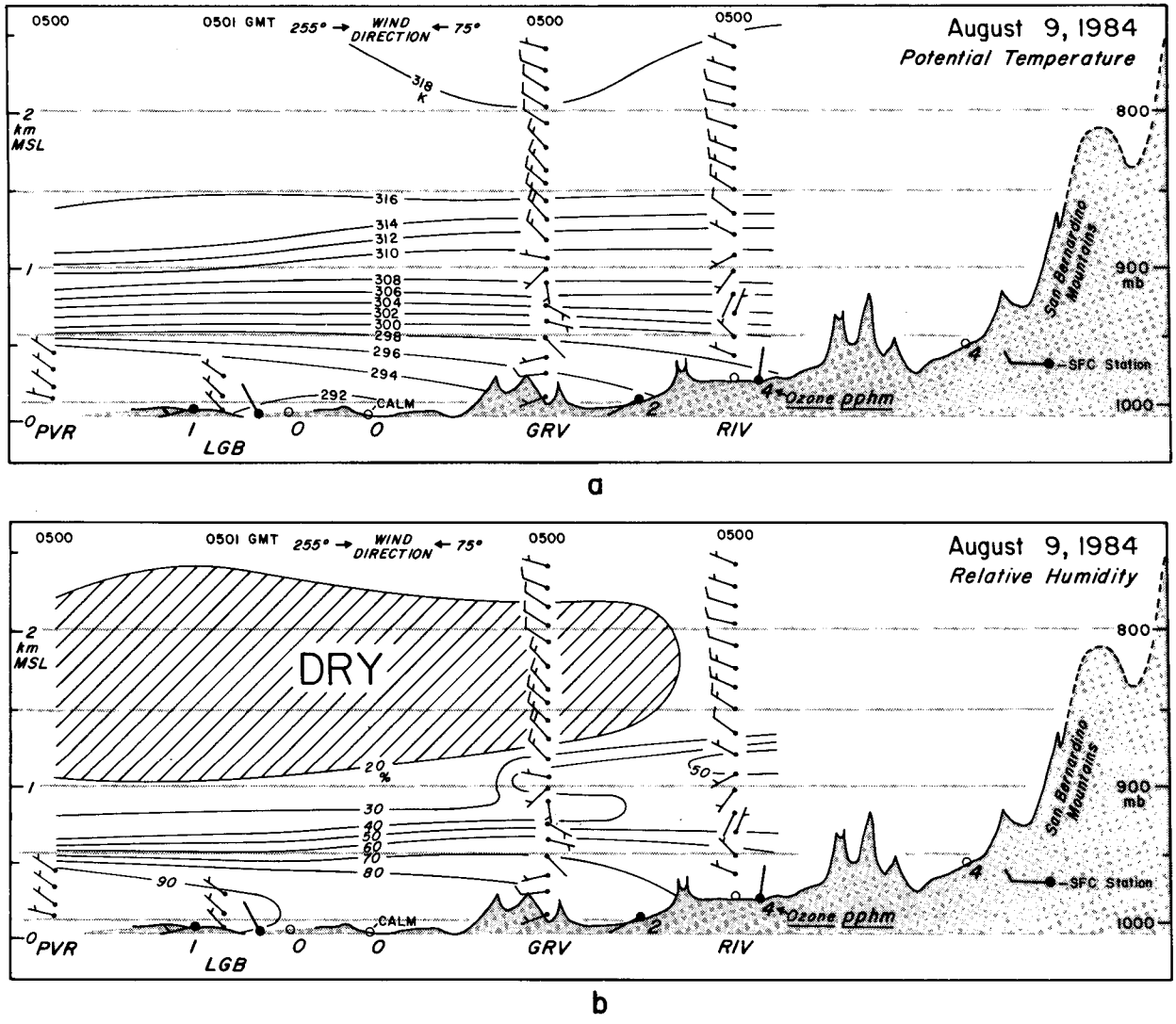

FIG. 9. As in Fig. 8 except for ~0500 GMT 9 August 1984.

between the 308 and 310 K isentropes which corresponds to a discontinuity in relative humidity over RIV and GRV. This humidity pattern suggests that the mixed layer was much deeper earlier in the day. In fact, an analysis at 2100 GMT 8 August (not shown) depicts a situation similar to Fig. 8a with the mixed layer being much deeper east of GRV, owing to the thermal convection from below. It is believed that an elevated pollution layer would have formed below ~310 K isentrope in the east part of the basin if the winds were not persistent from a westerly direction above the mixed layer.

5. Discussion and conclusions

Edinger (1973) and Blumenthal et al. (1978) both presented vertical cross sections of potential temperature from flight paths approximately over CWA, ELM, POM and RIV (see Figs. 1 and 2). Their results reveal high oxidant levels within the inversion, which they attribute to injection of pollutants in the vicinity of heated mountain slopes. The present study supports these works but also suggests that vertical mixing by thermals in the mixed layer, especially over the east basin, may contribute to the evolution of elevated pollution layers. In fact, several figures in both of the above mentioned studies suggest that large quantities of ozone may be forced aloft over the east basin by convective mixing before the advected, polluted air mass reaches the mountains. After combining with pollutants that are orographically forced aloft, elevated layers in both cases are advected westward within the stable layer toward the coastal areas. Naito et al. (1968), among others, has hypothesized that convective plumes are an important mechanism to transport pollution to higher levels in the atmosphere.

The apparent discontinuity in the depth of the mixed layer in the eastern basin over GRV and RIV during

the day (Figs. 7, 8, and 9) should not be surprising upon close examination of Fig. 2. The San Bernardino Riverside Valley is shielded from direct ocean effects except for the passes near the POM and GRV upper-air sites. During the day, heating at the surface is intense in this interior valley and results in a much deeper mixed layer. The findings suggest that at least two distinct boundary layer regimes must be considered over the Los Angeles area. Figure 10 summarizes how the combined effects of orography and convective mixing might produce elevated pollution layers over the east basin. The orographic effects include forced convection by upslope flow along the mountains (in the examples presented in this paper, this flow was a result of the sea breeze on 8 August and the Catalina Eddy on 9 and 10 August) or free convection owing to the heating of mountain slopes during the day. Convective mixing over a heated interior valley was well illustrated in section 4b.

Based on the analyses presented in this paper, it can be concluded that elevated pollution layers are a commonly observed phenomenon within the boundary layer in the Los Angeles area. It appears that upper-level winds within the inversion, orographic effects and thermally induced changes in the depth of the mixed layer control the evolution of these elevated layers. In addition to the results presented in this paper, it is believed that the depth of the mixed layer can be related to horizontal wind shear (or sea-breeze undercutting) which can lift the base of the inversion and redistribute pollutants to higher altitudes. It is important to incorporate these elevated pollution layers and the detailed airflow field in numerical modeling efforts since the aerosols can be reentrained into a deepening boundary layer at subsequent times near their origin or at other locales resulting in surface pollution concentrations that can be much higher than predicted. The modeling in turn is generally used for the development of strategies for the attainment and maintenance of the air quality standards.

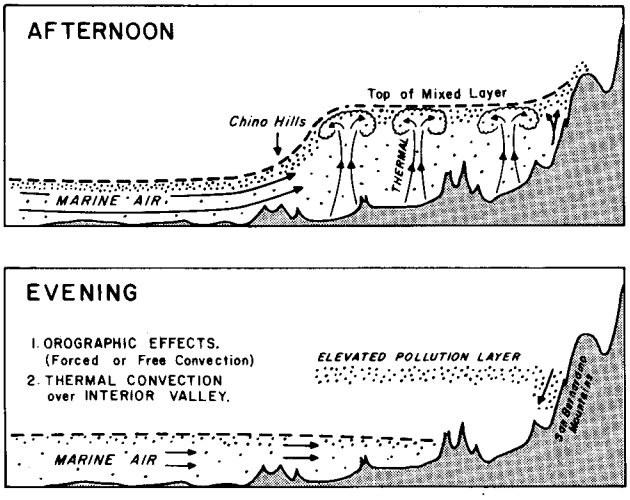

FIG. 10. Schematic model of the evolution of an elevated pollution layer over the east basin of Los Angeles. The elevated layer is hypothesized to form via two mechanisms shown in the Figure.

Acknowledgments. The authors are indebted to all the scientists involved with Project BASIN. One of the authors (RMW) is proud to acknowledge the cooperation of the faculty of the Department of Atmospheric Sciences at UCLA for allowing us to "borrow" their graduate students for balloon launches at the 11 upper-air sites. This research was sponsored by the California Air Resources Board under State of California Contract A3-104-32 (RMW), the South Coast Air Quality Management District under Contract HD840314 (RMW), and the U.S. Environmental Protection Agency (JLM). D. Landau and M. Beeson patiently reduced all of the BASIN upper-air data. The manuscript was typed by C. Wong.

REFERENCES

Angell, J. K., D. H. Pack, L. Machta, C. R. Dickson and W. H. Hoecker, Jr., 1972: Three-dimensional air trajectories determined from tetroon flights in the planetary boundary layer of the Los Angeles Basin. *J. Appl. Meteor.*, **11,** 451–471.

——, C. R. Dickson and W. H. Hoeker, Jr., 1975: Relative diffusion within the Los Angeles Basin as estimated from tetroon triads. *J. Appl. Meteor.*, **14,** 1490–1498.

——, —— and ——, 1976: Tetroon trajectories in the Los Angeles Basin defining the source of air reaching the San Bernardino-Riverside area in late afternoon. *J. Appl. Meteor.*, **15,** 197–204.

Beer, C., and L. B. Leopold, 1947: Meteorological factors influencing air pollution in the Los Angeles area. *Trans. Amer. Geophys. Union,* **28,** 173–192.

Blumenthal, D. L., W. H. White and T. B. Smith, 1978: Anatomy of a Los Angeles smog episode: Pollutant transport in the daytime sea breeze regime. *Atmos. Environ.*, **12,** 893–907.

Bosart, L. F., 1983: Analysis of a California Catalina Eddy event. *Mon. Wea. Rev.*, **111,** 1619–1633.

Collis, R. T. H., 1969: Lidar for routine meteorological observations. *Bull. Amer. Meteor. Soc.*, **50,** 688–694.

Cramer, O. P., 1972: Potential temperature analysis for mountainous terrain. *J. Appl. Meteor.*, **11,** 44–50.

——, and R. E. Lynott, 1961: Cross-sectional analysis in the study of windflow over mountainous terrain. *Bull. Amer. Meteor. Soc.*, **42,** 693–702.

Defant, F., 1951: Local winds. *Compendium of Meteorology,* Amer. Meteor. Soc., 655–672.

Dorman, C. E., 1985: Evidence of Kelvin Waves in California's marine layer and related eddy generation. *Mon. Wea. Rev.*, **113,** 827–839.

Drivas, P. J., and F. H. Shair, 1974: A tracer study of pollutant transport and dispersion in the Los Angeles area. *Atmos. Environ.*, **8,** 1155–1163.

Edinger, J., 1959: Changes in the depth of the marine layer over the Los Angeles Basin. *J. Meteor.*, **16,** 219–226.

——, 1963: Modification of the marine layer over coastal southern California. *J. Appl. Meteor.*, **2,** 706–712.

——, 1973: Vertical distribution of photochemical smog in Los Angeles Basin. *Environ. Sci. Technol.*, **7,** 247–252.

——, and R. Helvey, 1961: The San Fernando convergence zone. *Bull. Amer. Meteor. Soc.*, **42,** 626–635.

——, M. McCutchan, P. Miller, B. Ryan, M. Schroeder and J. Behar, 1972: Penetration and duration of oxidant air pollution in the south coast air basin of California. *J. Air Pollut. Control Assoc.*, **22,** 882–886.

Fosberg, M., 1967: Numerical analysis of convective motions over a mountain ridge. *J. Appl. Meteor.*, **6,** 889–904.

Hamilton, P. M., 1966: The use of lidar in air pollution studies. *Int. J. Air Water Pollut.*, **10,** 427–434.

Holzworth, G. C., E. Kauper and T. B. Smith, 1963: Some observed low-level air trajectories over Los Angeles, California. *Mon. Wea. Rev.*, **91,** 387–392.

Johnson, W. B., 1969: Lidar observations of the diffusion and rise of stack plumes. *J. Appl. Meteor.*, **8,** 443–449.

——, and E. E. Uthe, 1971: Lidar study of the Keystone stack plume. *Atmos. Environ.*, **5,** 703–724.

Kauper, E., 1960: The zone of discontinuity between the land and sea breezes and its importance to southern California air pollution studies. *Bull. Amer. Meteor. Soc.*, **41,** 410–422.

Lamb, B. K., A. Lorenzen and F. H. Shair, 1978: Atmospheric dispersion and transport within coastal regions—Part I. Tracer study of power plant emissions from the Oxnard plain. *Atmos. Environ.*, **12,** 2089–2100.

Lea, D. A., 1968: Vertical ozone distribution in the lower troposphere near an urban pollution complex. *J. Appl. Meteor.*, **7,** 252–267.

Malkus, J. S., 1955: The effects of a large island upon the trade-wind air stream. *Quart. J. Roy. Meteor. Soc.*, **81,** 538–550.

McElroy, J. L., 1982: Investigation of episodic air quality using airborne lidar. *Proc. Third Joint Conf. on Applications of Air Pollution Meteorology,* San Antonio, Amer. Meteor. Soc., 143–148.

——, 1985: Detection of pollutant dispersion in complex terrain by airborne lidar. *Proc. Seventh Symp. on Turbulence and Diffusion,* Boulder, Amer. Meteor. Soc., 240–243.

——, and T. B. Smith, 1986: Vertical pollutant distributions and boundary layer structure observed by airborne lidar near the complex southern California coastline. *Atmos. Environ.*, **20,** 1555–1566.

——, J. A. Eckert and C. J. Hager, 1981: Airborne down-looking lidar measurements during STATE 78. *Atmos. Environ.*, **15,** 733–743.

——, E. L. Richardson, W. H. Hawkins and M. J. Pearson, 1982: Airborne downward-looking lidar measurements during the South Coast Air Basin/southeast desert oxidant transport study. U.S. Environmental Protection Agency Rep. No. TS-AMD-82133, 74 pp. [Available from USEPA, Environmental Monitoring Systems Laboratory, Las Vegas, NV 89114.]

Melfi, S. H., J. D. Spinehirne, S. H. Chou and S. P. Palm, 1985: Lidar observations of vertically organized convection in the planetary boundary layer over the ocean. *J. Climate Appl. Meteor.*, **24,** 806–821.

Naito, K., I. Tabata and Y. Yokota, 1968: The vertical distribution of aerosol in the lower atmosphere observed by a lidar. *Pap. Meteor. Geophys.*, **19,** 615–625.

Neiburger, M., 1969: The role of meteorology in the study and control of air pollution. *Bull. Amer. Meteor. Soc.*, **50,** 957–965.

Orville, H. D., 1964: On mountain upslope winds. *J. Atmos. Sci.*, **21,** 622–633.

——, 1968: Ambient wind effects on the initiation and development of cumulus clouds over mountains. *J. Atmos. Sci.*, **25,** 385–403.

Pack, D. H., and J. K. Angell, 1963: A preliminary study of air trajectories in the Los Angeles Basin as derived from tetroon flights. *Mon. Wea. Rev.*, **91,** 583–604.

Robinson, E., 1952: Some air pollution aspects of the Los Angeles temperature inversion. *Bull. Amer. Meteor. Soc.*, **33,** 247–250.

Rosenthal, J., 1968: A Catalina eddy. *Mon. Wea. Rev.*, **96,** 742–743.

Russell, P. B., E. E. Uthe, F. L. Ludwig and N. A. Shaw, 1974: A comparison of atmospheric structure as observed with monostatic acoustic sounder and lidar techniques. *J. Geophy. Res.*, **79,** 5555–5566.

Schultz, P., and T. Warner, 1982: Characteristics of summertime circulations and pollutant ventilation in the Los Angeles basin. *J. Appl. Meteor.*, **21,** 672–682.

Shipley, S. T., E. V. Browell, D. S. McDougal, B. L. Orndorff and P. Haagenson, 1984: Airborne lidar observations of long-range transport in the free troposphere. *Environ. Sci. Technol.*, **18,** 749–756.

South Coast Air Quality Management District, 1985: Air quality summary. *Air Quality Digest,* Vol. 6, No. 5, 1–8. [South Coast Air Quality Management District, El Monte, CA 91731.]

Uthe, E. E., 1984: Cooling tower plume rise analyses by airborne lidar. *Atmos. Environ.*, **18,** 107–119.

——, and P. B. Russell, 1974: Experimental study of the urban aerosol structure and its relation to urban climate modification. *Bull. Amer. Meteor. Soc.*, **55,** 115–121.

——, and W. E. Wilson, 1979: Lidar observations of the density and behavior of the Labadie Power Plant plume. *Atmos. Environ.*, **13,** 1395–1412.

——, F. L. Ludwig and F. Pooler, 1980a: Lidar observations of the diurnal behavior of the Cumberland Power Plant plume. *J. Air Pollut. Control Assoc.*, **30,** 889–893.

——, N. B. Nielsen and W. L. Jimison, 1980b: Airborne lidar plume and haze analyzer (ALPHA—1). *Bull. Amer. Meteor. Soc.*, **61,** 1035–1043.

Wakimoto, R. M., and M. G. Wurtele, 1984: Project BASIN. *Bull. Amer. Meteor. Soc.*, **65,** 1210–1211.